Theoretical Investigation of the Oxidation of Propane by FeO+

ARTICLE *in* THE JOURNAL OF PHYSICAL CHEMISTRY A · FEBRUARY 2010

Impact Factor: 2.69 · DOI: 10.1021/jp910774z · Source: PubMed

4 AUTHORS, INCLUDING:

Zhaochun Liu
China University of Petroleum
45 PUBLICATIONS **85** CITATIONS

SEE PROFILE

Theoretical Investigation of the Oxidation of Propane by FeO^+

Zhaochun Liu,[†] Wenyue Guo,*[,†] Lianming Zhao,*[,†] and Honghong Shan[‡]

College of Physics Science and Technology and State Key Laboratory for Heavy Oil Processing, China University of Petroleum, Dongying, Shandong 257061, PR China

Received: November 12, 2009; Revised Manuscript Received: January 16, 2010

We report herein a comprehensive theoretical study of the oxidation of propane by FeO^+ on both the sextet and quartet potential energy surfaces (PESs) using density functional theory. The geometries and energies of all the stationary points involved are located. Interaction of FeO^+ with propane could account for four types of encounters (i.e., α,β,γ-, $2\alpha,\beta$-, 3α-η^3, and $2\alpha,2\gamma$-η^4) complexes. Various mechanisms leading to the loss of CH_3, H_2O, C_3H_7OH ($H_2O + C_3H_6$), and C_3H_6 are analyzed in terms of the topology of the PES. The reaction of FeO^+ with propane involves initial C−H activation, while initial C−C activation is indeed unlikely to be important. The loss of CH_3 takes place adiabatically on the sextet PES via the simple C^α-to-O H shift from η^4-$OFe^+(C_3H_8)$ followed by CH_3 shift. The C_3H_7OH elimination proceeds via direct C^α-to-O H shift followed by C−O coupling, while the loss of H_2O, C_3H_6, and ($H_2O + C_3H_6$) proceeds via the α,β-H and β,α-H abstraction mechanisms from all the η^3 complexes. The most favorable channel is the α,β-H abstraction mechanism for the H_2O loss because it not only is energetically and dynamically favorable but also has a high crossing probability between the sextet and quartet PESs. The computational results are in concert with the available experimental information and add new insight into the details of the individual elementary steps.

Introduction

In view of enormous practical importance in industrial and environmental processes, reactions catalyzed by transition metal ions have attracted great interest.[1] In modern catalytic chemistry, selective catalytic oxidation of hydrocarbons is one of the most important subjects.[2,3] In this respect, gas-phase experiments combined with theoretical works provide a wealth of insight into elementary steps and reactive intermediates for various catalytic reactions.[4,5] Transition metal oxide ions usually play a key role in catalytic oxidation of alkane with transition metal ions.[3–9] Oxidations of propane by transition metal oxides in the gas phase have been investigated extensively.[3,6–9] Results of ion beam reactive scattering techniques suggested that reaction of CrO^+ with propane yields hydrogen, ethane, propene, and C_3H_8O.[8] The Fourier transform ion cyclotron resonance (FT-ICR) study showed that reaction of CoO^+ with propane accounts for the dominant products of $Co(C_3H_6)^+$ and Co^+, accompanying with fewer $Co(C_2H_4)^+$ and $Co(H_2O)^+$.[9] Loss of methyl radical is also prominent in the reaction of MnO^+ with propane.[7] By using Fourier transform mass spectroscopy (FTMS), Jackson et al. reported that FeO^+ reaction with propane gives propene (10%), water (50%), and propanol (20%).[6] In addition, a new channel (20%) giving the loss of methyl radical in the FeO^+/C_3H_8 system yields a species of composition $[Fe, C_2, H_5, O]^+$.

For the sake of unveiling the reaction mechanisms, several theoretical studies on the hydroxylation reactions of hydrocarbons with transition metal oxide ions have been reported.[10–12] The reaction pathway for the direct methane-to-methanol conversion mediated by MO^+ (M = Fe, Co, and Ni) was reported to proceed via a direct H abstraction to form intermediate CH_3-M^+-OH followed by a methyl migration.[11] Yoshizawa et al. have reported that the direct oxidation of benzene to phenol by FeO^+ contains three different mechanisms: nonradical, radical, and oxygen insertion.[10,11e,12a] The major reaction pathway favors the nonradical mechanism to form a hydoroxo intermediate, $HO-Fe^+-C_6H_5$, via H-atom abstraction with a four-member-ring transition state as the rate-determining barrier.[11e,12a] Recently, we carried out a theoretical investigation on the Fe^+-catalyzed oxidation of acetylene by N_2O using density functional theory (DFT).[13] Our results explicitly explained both two-step and three-step catalytic cycles.

Nevertheless, to the best of our knowledge, so far, quantum-chemical studies of the saturated alkanes oxidation by MO^+ are rather scarce.[11,12b–g] In this article, we report a comprehensive theoretical study of propane oxidation by FeO^+. One important reason for this study is iron ion was found to present a good reactivity both experimentally and theoretically.[3,5,6,13] Second, this reaction may involve C−H and/or C−C activations. Last, propane reaction with transition metal oxide ions has been paid much attention,[3,6–9] because it is the smallest alkane for which exothermic reactions are observed at thermal energies.[14] The aim of this paper is to illustrate the reaction mechanisms and activation barriers useful to give insight into the kinetic aspects for the reaction of FeO^+ with propane. This includes a complete illustration of all possible pathways for producing products via C−C and C−H activations on both the sextet and quartet PESs as well as an estimation of the crossing possibility between the high- and low-spin surfaces where it is needed. Indeed, spin inversion has been suggested to play an important role in the reaction of small organic molecules with transition metal ions, such as Fe^+, Co^+, Ni^+, etc.[11c,13,15,16]

2. Computational Details

The three-parameter hydbrid B3LYP functional[17] together with the DZVP(opt+3f)[13,18] for Fe^+ and 6-311++G(2d,2p) basis

* Corresponding author. E-mail: W.G., wyguo@upc.edu.cn; L.Z., lmzhao2008@yahoo.com.cn).
[†] College of Physics Science and Technology.
[‡] State Key Laboratory for Heavy Oil Processing.

10.1021/jp910774z
Published on Web 02/03/2010

set[19] for nonmetal atoms (noted as BSI for the basis sets) was employed in the structural optimization for all the reactants, products, intermediates, and transition states involved in the title reaction. The DZVP(opt) sets built up by Chiodo et al. have presented a good reliability for the density functional B3LYP method in predicting transition metal ion ground- and excited-state order and splitting.[13,18,20] In a recent work,[13] we have shown the performance of this computational strategy for describing the features of the PESs of the $Fe^+/N_2O/C_2H_2$ system. Furthermore, our calculation also reproduced the experimental bond dissociation energy (BDE) of $^4[Fe^+-C_3H_6]$ well (36.5 vs 37.0 kcal/mol).[21]

Vibrational analysis was performed to characterize all stationary points on the PESs as local minima or transition states and to evaluate the zero point energies (ZPE) included in all energies reported. Intrinsic reaction coordinate (IRC) calculations[22] were performed to identify the pathways between transition states and their relevant minima. The calculation method STABLE[23] was used everywhere to ensure the wave function of stationary points to be tested. Natural bond orbital (NBO)[24] analyses were carried out to characterize the bonds and the interactions inside some important species.

To locate the minimum energy crossing point (MECP) between the sextet and quartet surfaces for a step considered, single-point energies of both states were calculated at the B3LYP/BSI level for the relevant IRC points along the quartet pathway until they reached an equal energy. All these calculations were performed using the Gaussian 03 package.[25]

Spin−orbit coupling (SOC) at the MECP was calculated with the GAMESS package.[26] CASSCF calculations with the DZVP(opt+3f) basis set[18] for Fe, and the 6-311G basis for the remaining atoms were first performed for both states at the MECP to get the converged CASSCF wave functions, the SOC matrix elements were then computed using the SOC−CI method.[27] Because the orbital sets of the two states must share a common set of frozen core orbitals in the SOC matrix elements calculations, the converged CASSCF quartet wave functions were employed as a reference state for both the sextet and quartet CI wave functions. The one-electron effective spin−orbit operator was used as eq 1,[27]

$$\mathbf{H}_{SO} = \frac{\alpha^2}{2}\sum_i \sum_k \left(\frac{Z_k^*}{r_{ik}^3}\right)\mathbf{S}_i \cdot \mathbf{L}_{ik}$$

$$\frac{\alpha^2}{2} = \frac{e^2 h}{4\pi m_e^2 c^2} \qquad (1)$$

where $\mathbf{L}_{ik}$ amd $\mathbf{S}_i$ are the orbital and spin angular momentum operators, respectively, for electron i in the framework of nuclei indexed by k. The effective nuclear charge Z_k^* is an empirical parameter in the one-electron spin−orbit Hamiltonian. Z^* is 3.9, 5.6, and 13.9 for carbon, oxygen, and iron, respectively.[28]

The SOC value is the matrix element that expresses the coupling of the sextet and quartet states by the operator of eq 2,

$$\langle \mathbf{H}_{SO} \rangle_{S,S'} = \langle {}^6\Psi_1(\mathbf{M}_S)|\mathbf{H}_{SO}|{}^4\Psi_2(\mathbf{M}_{S'})\rangle \qquad (2)$$

Here $^6\Psi_1$ ($^4\Psi_2$) is the $\mathbf{M}_S$ ($\mathbf{M}_{S'}$) component of the many-body sextet-state (quartet-state) wave function. Considering the generated spin sublevels $\mathbf{M}_S$, a reasonable measure of the SOC-induced sextet-quartet interaction is the root-mean-square coupling constant (SOCC) of eq 3,

$$\mathrm{SOCC} = [\sum_{S,S'} \langle \mathbf{H}_{SO} \rangle_{S,S'}{}^2]^{1/2} \qquad (3)$$

A crude estimation of the crossing probability at the MECP can be done using the Landau−Zener formula,[29]

$$P = 1 - e^{-2\delta}$$

$$\delta = \frac{\pi |V_{ij}|^2}{\hbar v |\Delta g_{ij}|} = \frac{\pi |\mathrm{SOCC}|^2}{(2\min(S_i,S_j)+1)\hbar v |\Delta g_{ij}|} \qquad (4)$$

where V_{ij} is the matrix element of a diabatic operator (SOC in this case) coupling two adiabatic states i and j, Δg_{ij} is the difference in the gradients of the two adiabatic states i and j, and v is the effective velocity with which the system is passing through the crossing point that can be calculated from the kinetic theory of gases at 298 K.

3. Results and Discussion

In the following sections, we will first give the structures and energies of encounter complexes and product species involved in the title reaction. Then, we will examine the reaction in detail, including geometries of various stationary points, PES profiles for all possible product channels, as well as intersystem crossing possibilities for some relevant steps. Last, we will give the reaction mechanisms by comparing our theoretical results with the experimental findings.[6] For simplicity, calculated total energies, zero point energies, and $\langle S^2 \rangle$ values for all the species involved are given as Supporting Information (see Table S1).

3.1. Encounter Complexes and Product Species. In this section, we discuss calculated structures and energies for encounter complexes and product species relevant to the $FeO^+ + C_3H_8$ reaction. Figure 1 shows the optimized geometries as well as selected structural parameters for these complexes. Table 1 tabulates the BDEs of $OFe^+-C_3H_8$.

All possible complexes of FeO^+ with C_3H_8 are considered, and four types of encounter isomers, i.e., **1a**−**1d**, are found on the PESs of $[O, Fe, C_3, H_8]^+$. **1a**, **1b**, and **1c** are η^3-$OFe^+-C_3H_8$ complex, in which Fe^+ of FeO^+ is simultaneously coordinated to α,β,γ-, 2α,β-, and 3α-H atoms (noted as α,β,γ-, 2α,β-, and 3α-η^3 complexes), respectively; bonding to FeO^+ results in the stretching of the adjacent C−C and C−H bonds in C_3H_8 by 1.1−1.6% and 1−3.8%. **1d** is featured by an η^4-$OFe^+-C_3H_8$ complex (two α-H and two γ-H; noted as 2α,2γ-η^4 complex), in which the C−C bond lengths change slightly. Quartet minima ^{4}**1a**, ^{4}**1b**, ^{4}**1c**, and ^{4}**1d** have the C_s, C_1, C_s, and C_{2v} symmetries, respectively; whereas ^{6}**1c** has C_s symmetry and the others (^{6}**1a**, $_6$**1b**, and ^{6}**1d**) possess the overall C_1 symmetry.

As shown in Table 1, the binding energies of complexes **1a**−**1d** are between 31.1−36.7 (sextet) and 25.6−33.6 (quartet) kcal/mol, indicating the nearly identical stability as well as the coexistence for these isomers in the gas phase. We can also find that the stabilities of the complexes depend on their structures, i.e., the 3α-η^3 complex accounts for the weakest binding, while the η^4 complex affords the strongest binding. The different stabilities of the complexes can be explained by the extent of electron transfer between the FeO^+ entity and the adjacent nucleophilic σ bonds in C_3H_8. NBO analysis shows the association of $OFe^+-C_3H_8$ (**1a**−**1d**) is dominated by

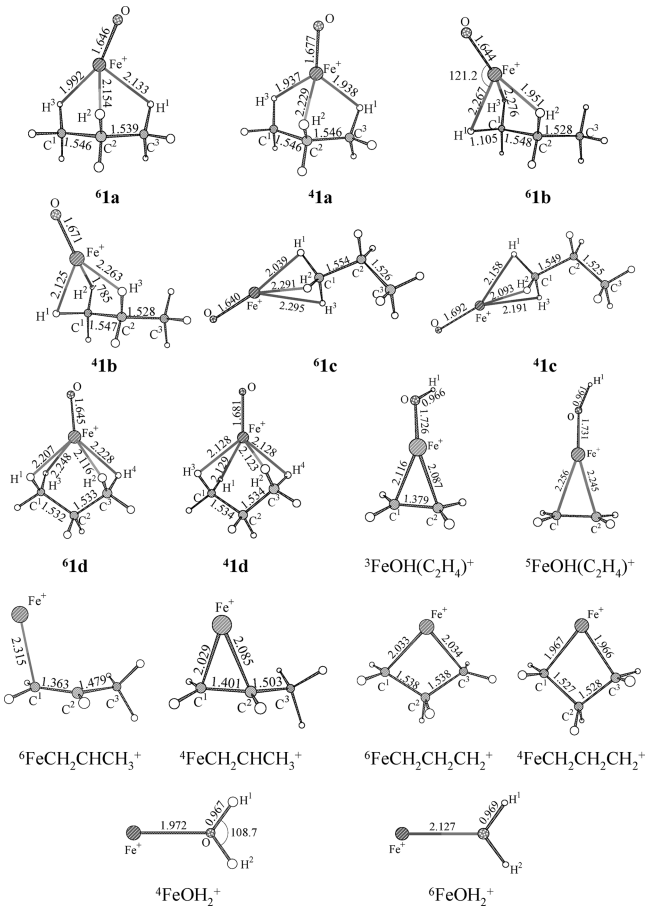

Figure 1. Geometries and selected structural parameters optimized at the B3LYP/DZVP(opt+3f)+6-311++G(2d,2p) level for encounter complexes, product species involved in the FeO^+ + propane reaction. Bond lengths are in angstroms, and bond angles are in degrees.

TABLE 1: Calculated Bond Dissociation Energies BDE (in kcal/mol) of FeO^+ with Propane at the B3LYP/DZVP(opt+3f)+6-311+G(2d,2p) Level[a]

	BDE	
species	sextet	quartet
1a	34.5	31.6
1b	33.1	30.4
1c	31.1	25.6
1d	36.7	33.6

[a] Energies are relative to the total energy of FeO^+ ($^6\Sigma^+$) and propane.

electrostatic interaction as well as donor−acceptor stabilization, in which electrons are mainly donated from the adjacent σ(C−H) and σ(C−C) orbitals to the unoccupied 4s3d(Fe^+) and σ^*(Fe^+−O) orbitals ($E^{(2)}$ = 38.0 (51.0) (**1a**), 29.8 (37.7) (**1b**), 25.6 (28.7) (**1c**), and 38.6 (50.6) (**1d**) in the sextet (quartet) state). Note that the donor−acceptor stabilizations indeed follow the same order as the BDEs for the encounter complexes (with the exception of ^{4}**1a** and ^{4}**1d**). Furthermore, ^{4}**1a**, ^{4}**1b**, and ^{4}**1d** favor much stronger donor−acceptor interaction than its sextet analogues, whereas the donor−acceptor stabilization of ^{4}**1c** is only 2.9 kcal/mol larger than that of ^{6}**1c**. As a result, although FeO^+($^4\Pi$) is located 8.1 kcal/mol above FeO^+($^6\Sigma^+$), the energy gap between the quartet and sextet states decreases to 5.5 kcal/mol for **1c**, and only about 3 kcal/mol for **1a**, **1b**, and **1d**.

$FeOH(C_2H_4)^+$ is the major product via methyl elimination in the title reaction (see Figure 1).[6] One striking feature of the product is the dicoordination of the metal with the OH and C_2H_4 groups. For both multiplicities, the Fe^+−C distances are calculated to be longer than 2 Å, compared to the relatively short Fe^+−O bond length (about 1.73 Å; see Figure 1). NBO analysis detects that binding in the Fe^+−(C_2H_4) moiety is primarily electrostatic in character: electron donation from the π(C−C) orbital to the unoccupied 4s3d(Fe^+) and σ^*(Fe^+−O) orbitals ($E^{(2)}$ = 43.3 (quintet) and 58.7 (triplet) kcal/mol) as well as the back-donation from the occupied 3d(Fe^+) orbital to the π^*(C−C) orbital ($E^{(2)}$ = 8.7 (quintet) and 20.8 (triplet) kcal/mol). In the fragment complex Fe^+−OH, however, iron ion and hydroxyl are covalently bound via the formation of the β-singly occupied σ(Fe^+−O) and π(Fe^+−O) bonding orbitals in the quintet state and the α-singly occupied σ(Fe^+−O) bonding orbital on the triplet PES. The relatively strong covalent interaction of HO−$Fe^+C_2H_4$ in the quintet state explains the much larger stabilization in this state (quintet → triplet excitation energy: 24.0 kcal/mol).

$FeOH_2^+$ is the propene-elimination product in the reaction of FeO^+ with propane.[6] While the quartet BDE is only slightly larger than that of the sextet (33.0 vs 32.0 kcal/mol), the bond length of $^4Fe^+$−OH_2 (2.127 Å) is obviously shorter than its sextet analogue (1.972 Å). NBO analysis suggests that the species is stabilized by electron donations from the 2s2p(O) lone pair orbital to the unoccupied 4s3d(Fe^+) orbitals in both states ($\Delta E^{(2)}$ = 17.5 (sextet) and 30.4 (quartet) kcal/mol). In addition, the sextet species also favors a back-donation of 4s(Fe^+) → 3s(O) ($\Delta E^{(2)}$ = 6.6 kcal/mol), explaining the comparable BDEs between the high and low states. Note that the calculated BDE of ^{4}[Fe^+−OH_2] agrees well with the experimental value (30.7 kcal/mol).[30]

For the H_2O elimination product,[6] two candidates can be envisaged: $FeCH_2CHCH_3^+$ complex via α,β-H abstraction and *quadrilateral*-type $FeCH_2CH_2CH_2^+$ complex via α,γ-H abstraction (see Figure 1). The sextet $FeCH_2CHCH_3^+$ complex is featured by the attachment of the metal to the methene-C atom of CH_2CHCH_3, whereas the quartet counterpart favors an alkenyl-CC π-type bound structure. In the sextet and quartet states, the BDEs are calculated to be 30.7 and 48.4 kcal/mol, suggesting that the π-type bonding indeed largely stabilizes the species. NBO analysis shows that the complex is stabilized by the classical Dewar−Chatt−Duncanson mechanism,[31] i.e., donation of 3d(Fe^+) → π^*(CC) ($\Delta E^{(2)}$ = 7.6 (sextet) and 56.9 (quartet) kcal/mol) and back-donation of π(CC) → 4s(Fe^+) ($\Delta E^{(2)}$ = 25.6 (sextet) and 58.6 (quartet) kcal/mol). Furthermore, because of the electrostatic repulsion between the diffused 4s(Fe^+) electron and CH_3, the metal is far away from the methyl end in the sextet species. The *quadrilateral*-type Fe^+−$CH_2CH_2CH_2$ is formed because Fe^+ simultaneously attacks at both terminal C atoms of $CH_2CH_2CH_2$ with the Fe^+−C distances of 2.034 Å for the quartet and 1.967 Å for the sextet. Energetically, the quartet species is 20.3 kcal/mol more stable than the sextet analogue. NBO analysis suggests that only the β singly occupied σ(Fe^+C^1) and doubly occupied σ(Fe^+C^3) bonding orbitals are formed in the sextet $FeCH_2CH_2CH_2^+$, and the larger stability of the quartet species results from the two doubly occupied σ(Fe^+C) bonding orbitals.

3.2. Gas-Phase Reaction Mechanisms. Propane oxidation by FeO^+ in the gas phase could result in four neutral eliminations corresponding to H_2O, CH_3, C_3H_7OH (or H_2O + C_3H_6), and C_3H_6, as observed in ref 6. In the following, we consider all possible mechanisms for the propane oxidation: initial C−C

TABLE 2: Summary of All the Possible Products and the Reaction Energies *E* (in kcal/mol) Associated with the Reaction of FeO^+ with Propane at the B3LYP/DZVP(opt+3f)+6-311+G(2d,2p) Level[a]

products	*E* sextet	*E* quartet
$FeOH(C_2H_4)^+ + CH_3$ (**P$_{1a}$**)	−36.1	−12.1
$FeO(C_2H_5)^+ + CH_3$ (**P$_{1b}$**)	20.3	33.8
$FeCH_3(OH)^+ + C_2H_4$ (**P$_{1a'}$**)	−28.2	−31.5
$FeCH_3(C_2H_4)^+ + OH$ (**P$_{1b'}$**)	−0.4	13.2
$Fe^+ + C_3H_7OH$ (**P$_{2a}$**)	−13.8	−1.5
$Fe^+ + CH_2CHCH_3 + H_2O$ (**P$_{2b}$**)	−9.7	2.6
$Fe^+ + c\text{-}C_3H_6 + H_2O$ (**P$_{2c}$**)	0.9	13.2
$FeOH_2^+ + CH_2CHCH_3$ (**P$_{3a}$**)	−41.7	−42.7
$FeOH_2^+ + c\text{-}C_3H_6$ (**P$_{3b}$**)	−31.1	−32.1
$FeCH_2CHCH_3^+ + H_2O$ (**P$_{4a}$**)	−40.4	−58.1
$FeCH_2CH_2CH_2^+ + H_2O$ (**P$_{4b}$**)	−15.3	−35.6

[a] Energies are relative to the total energy of FeO^+ ($^6\Sigma^+$) and propane.

activation, C^α−H activation, and C^β−H activation. Table 2 tabulates all possible products as well as reaction energies for these observed eliminations (products **1a** through **4b**) and the unobserved products (**1a′** and **1b′**) for comparison.

3.2.1. Initial C−C Activation. PES together with schematic structures involved in the sextet and quartet pathways of the channel is shown in Figure 2. Information about the relevant species is given in Figure S1 (Supporting Information). This channel involves encounter complex **1a** (α,β,γ-η^3 complex). Starting from **1a**, the iron metal inserts into a C−C bond of propane to form species **2** ($CH_3Fe^+(O)CH_2CH_3$), which in its sextet and quartet states lies at +2.3 and −21.8 kcal/mol, respectively, with respect to the energetic zero. For both multiplicities, NBO analysis indicates that Fe^+ forms strong covalent bonds with CH_3, O, and CH_2CH_3, accounting for a tricoordinated structure of the new species. Transition state (**TS$_{1a-2}$**) for this possibility on the respective sextet and quartet pathways lies at +0.6 and −7.0 kcal/mol. It should be pointed out that the B3LYP/BSI calculation finds ^{6}**2** to be a true minimum, though it is energetically placed slightly above ^{6}**TS$_{1a-2}$** due to the ZPE effect. Direct dissociation of **2** could account for the CH_3 loss product $OFe^+(C_2H_5)$ (**P$_{1b}$**); however, it is strongly endothermic on both PESs (at least 20.3 kcal/mol).

A subsequent β-H shift to the oxygen atom produces the product-like intermediate (**3**), which largely stabilizes the system (E_{rel} = −57.2 and −68.9 kcal/mol on the sextet and quartet PESs, respectively). The new species can also be explained as the tricoordination of Fe^+ (with the CH_3, OH, and CH_2CH_2 groups). Another striking feature of the species is the CC π-type bound structure of the metal with C_2H_4. NBO analysis suggests that the metal center forms strong covalent bonds with OH and CH_3 via β-singly occupied $\sigma(Fe^+O)$ and $\pi(Fe^+O)$ and doubly occupied $\sigma(Fe^+C)$ bonding orbitals, whereas the binding of $Fe^+-C_2H_4$ is dominated by donor−acceptor stabilization ($\Delta E^{(2)}$ = 73.8 (quartet) and 40.6 (sextet) kcal/mol). The relevant transition state (**TS$_{2-3}$**), lying at 3.4 (4.9) kcal/mol on the quartet (sextet) PES, constitutes the highest energy point along the whole C−C activation reaction coordinate. Species **3** could undergo direct bond cleavage giving products CH_3 + $FeOH(C_2H_4)^+$ (**P$_{1a}$**), $FeCH_3(OH)^+ + C_2H_4$ (**P$_{1a'}$**), and $FeCH_3(C_2H_4)^+ + OH$ (**P$_{1b'}$**), with the reaction energies of −36.1 (−12.1), −28.2 (−31.5), and −0.4 (13.2) kcal/mol, respectively, in the quartet (sextet) state.

By observing the high- and low-spin PESs, we can find that this product channel experiences a common crossing immediately before the C−C insertion transition state (**TS$_{1a-2}$**). However, the rate-limiting barriers (**TS$_{2-3}$**) on both PESs are highly located above the energetic zero (E_{rel} = 4.9−3.4 kcal/mol). Thus, the initial C−C insertion is unlikely to be important for the reaction of FeO^+ with propane, in accordance with the fact that no OH and especially ethylene loss products were observed in the ICR experiment.[6]

3.2.2. Initial C−H Activation. The reaction pathways along the initial and sebsequent C−H bond activation branch involves three possible channels, that is, (i) α,β-H abstraction, (ii) α,γ-H abstraction, and (iii) β,α-H abstraction. In the following, we consider these channels.

α,β-H Abstraction. The sextet and quartet PESs together with the schematic structures involved in the reaction channel are shown in Figure 3. Information about the relevant species is given in Figures S2 (sextet) and S3 (quartet) (Supporting Information).

This channel involves encounter complexes **1b** and **1c** ($2\alpha,\beta$- and $3\alpha-\eta^3$ complexes). Through concerted, metal mediated C^α-to-O hydrogen shift, both complexes could give birth to hydroxyl complex $(HO)Fe^+(CH_2CH_2CH_3)$ (**4**), which is featured by a dicoordination structure of the metal center. NBO analysis detects that in both states Fe^+ forms strong covalent bonds with OH and $CH_2CH_2CH_3$ via doubly occupied $\sigma(Fe^+-C)$ and β-singly occupied $\sigma(Fe^+-O)$ and $\pi(Fe^+-O)$ bonding orbitals, leading to a large stability of the new species (E_{rel} = −54.5 (−58.5) kcal/mol in the sextet (quartet) state). The transition states for this possibility (**TS$_{1b-4}$** and **TS$_{1c-4}$**) are located at 5.0−16.0 kcal/mol below the energetic zero.

As shown in Figure 3, a sextet-to-quartet crossing is expected to occur just before saddle points **TS$_{1b-4}$** and **TS$_{1c-4}$**. The activated C^α−H bond of the relevant MECP (**MECP$_{1b}$**) involved in the energetically favorable **1b** → **TS$_{1b-4}$** process is slightly stretched to 1.138 Å (see Figure S3, Supporting Information), suggesting it is indeed an "early" crossing point. The SOCC is found to be 376.6 cm^{-1}, and the intersystem crossing probability is estimated to be 74% at room temperature, suggesting the spin-inversion occurring earlier in this process indeed plays a very important role in the reaction mechanism.

Once $(HO)Fe^+(CH_2CH_2CH_3)$ (**4**) is formed, two possible pathways would be immediately followed, i.e., C−O coupling and β-H transfer. In the following, we will discuss them one by one.

As seen in Figure 3, C−O coupling between OH and $CH_2CH_2CH_3$ in species **4** could result in the Fe^+−propanol adduct (**5**), the direct precursor of the propanol loss products. The relevant transition state (**TS$_{4-5}$**) is located at −26.6 (sextet) and −30.9 (quartet) kcal/mol, respectively. A striking feature of the new species is the attachment of the metal to the O atom of propanol with the Fe^+−O distance of 2.038 (sextet) and 1.933 (quartet) Å. NBO analysis shows that the adduct is stabilized to some extent by electron donation from the 2s2p(O) lone pair orbital to the unoccupied 4s3d(Fe^+) orbitals ($\Delta E^{(2)}$ = 20.7 (sextet) and 36.7 (quartet) kcal/mol). Species **5** (E_{rel} = −56.6 and −58.1 kcal/mol) has almost the same stability as precursor **4** in both the sextet and quartet states. Finally, direct dissociation of $Fe^+-(CH_3CH_2CH_2OH)$ would account for the loss of propanol and Fe^+(^{6}D or ^{4}F) (**P$_{2a}$**), with the overall exothermicity of 13.8 or 1.5 kcal/mol.

The other exit of species **4** involves β-H shift to the metal giving hydride-containing species $(C_3H_6)Fe^+(H)(OH)$ (**6**), which lies at −49.7 (sextet) and −60.8 (quartet) kcal/mol. Similar to

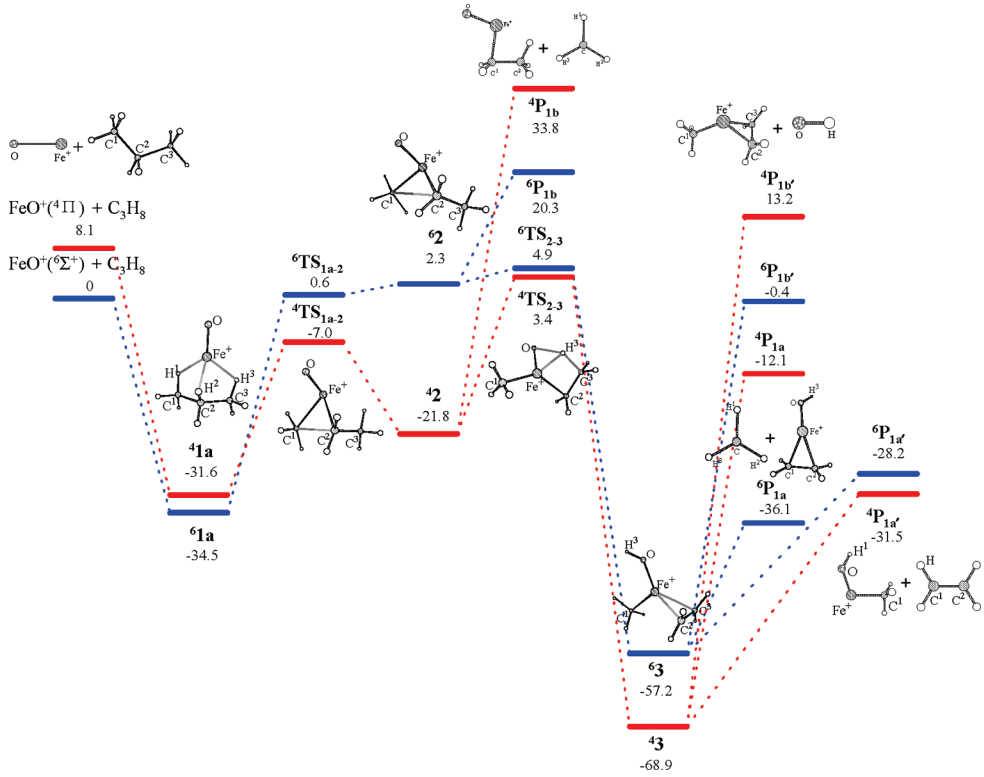

Figure 2. Energy profile the initial C−C activation channel involved in the reaction of FeO^+ with propane. Numbers refer to the relative stabilities (in kcal/mol) with respect to the separated reactants of $FeO^+(^6\Sigma^+)$ + propane evaluated at the B3LYP/DZVP(opt+3f)+6-311++G(2d,2p) level including ZPE corrections. The scaling factor for the ZPE is 0.961.

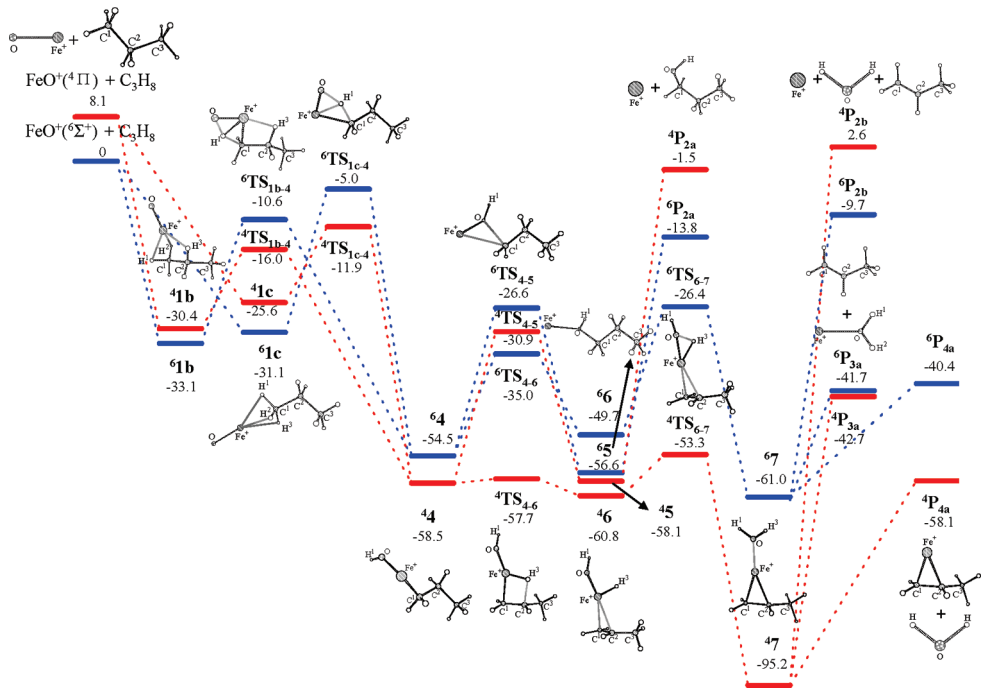

Figure 3. Energy profile for the initial C−H activation channel following α,β-H abstraction involved in the reaction of FeO^+ with propane. Parameters follow the same notations as in Figure 2.

both **2** and **3**, the new species is also featured by a tricoordination of the metal with H, OH, and CH_2CHCH_3. This possibility involves transition state $\mathbf{TS_{4-6}}$, lying at −35.0 and −57.7 kcal/mol in its sextet and quartet states.

A subsequent hydride-H shift from species **6** accounts for complex $(C_3H_6)Fe^+(OH_2)$ (**7**), the direct precursor of the H_2O-loss products. The relevant transition state ($\mathbf{TS_{6-7}}$) in its sextet and quartet states is located at −53.3 and −26.4 kcal/mol. The new species can be explained as dicoordination of the metal center (with H_2O and CH_2CHCH_3). Furthermore, it is also featured by a CC π-type bound structure of Fe^+ with CH_2CHCH_3. NBO analysis suggests that the binding of Fe^+ with

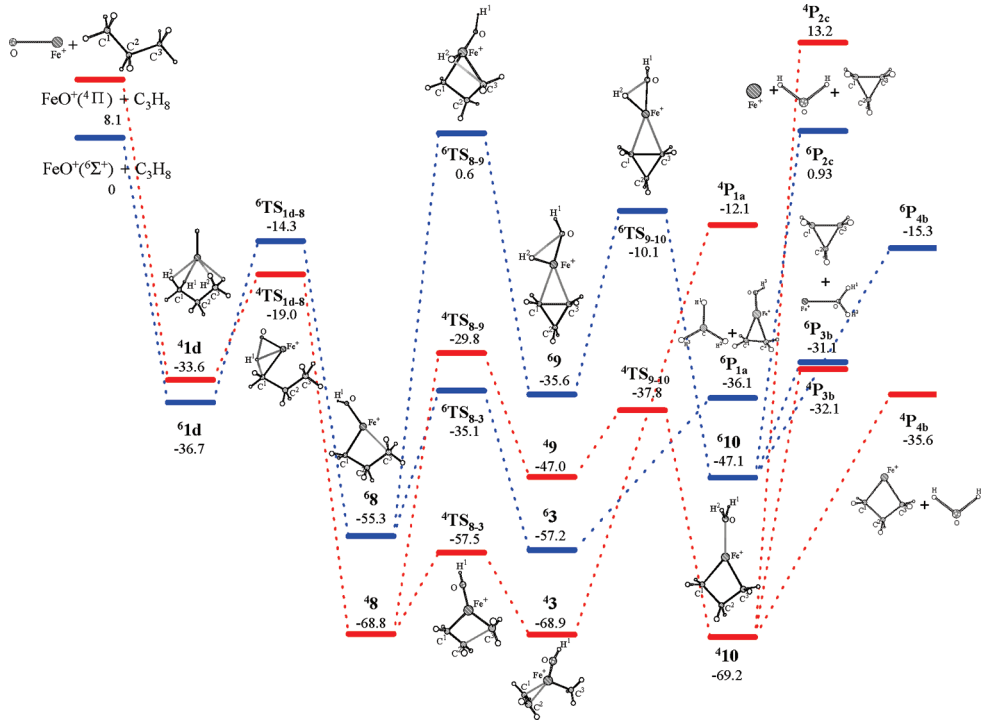

Figure 4. Energy profile the initial C−H activation channel following α,γ-H abstraction involved in the reaction of FeO^+ with propane. Parameters follow the same notations as in Figure 2.

the C_3H_6 and H_2O groups is dominated by relatively weak donor−acceptor stabilization in the sextet species ($\Delta E^{(2)} = 28.3$ and 44.8 kcal/mol) due to the singly occupation of the diffuse 4s orbital (natural charge population: $4s^{1.02}3d^{6.04}$), while the quartet complex favors much strong electron transfer from Fe^+ to both C_3H_6 and H_2O ($\Delta E^{(2)} = 42.0$ and 120.6 kcal/mol). These facts explain the relative short distances between Fe^+ and ligands (see Figure S3, Supporting Information) as well as the strong stability of the quartet species (lying at −95.2 kcal/mol or being 34.2 kcal/mol more stable than ^{6}**7**). Indeed, the new quartet species constitutes the deepest energy well on the whole PES.

Direct dissociation of species **7** could account for $Fe^+ + CH_2CHCH_3 + H_2O$ (**P$_{2b}$**), $FeOH_2^+ + CH_2CHCH_3$ (**P$_{3a}$**), and $FeCH_2CHCH_3^+ + H_2O$ (**P$_{4a}$**) with the overall exothermicities of 9.7 (−2.6), 41.7 (42.7), and 40.4 (58.1) kcal/mol, respectively, in the sextet (quartet) states.

α,γ-H Abstraction. PES together with schematic structures involved in the sextet and quartet pathways of the channel is shown in Figure 4. Information about these relevant species is given in Figure S4 (Supporting Information). We can find that this channel starts with the formation of encounter complex **1d** (2α,2γ-η^4 complex). Along this pathway, methyl-H migration to the oxide O could carry species **1d** to hydroxyl intermediate **8**, which stabilizes the system largely (E_{rel} = −55.3 (sextet) and −68.8 (quartet) kcal/mol). Different from the analogous hydroxyl species **4** ((HO)$Fe^+(CH_2CH_2CH_3)$), species **8** is strikingly featured by simultaneous attachment of Fe^+ to both the terminal CH_2 and CH_3 groups of $CH_2CH_2CH_3$ forming a ring structure (see Figure 1), explaining the large stability of the species. Transition state (**TS$_{1d-8}$**) for this process is located at −14.3 (−19.0) kcal/mol in the sextet (quartet) state.

The fact that the quartet state of **TS$_{1d-8}$** is more stable than its sextet state indicates a crossing between the high- and low-spin surfaces should occur before the saddle point. The relevant MECP (MECP$_{1d}$) is located at a geometrical structure very similar to species **1d** (see Figure S4, Supporting Information), suggesting an early crossing point is involved. The spin−orbit coupling constant (SOCC) is calculated to be 31.8 cm^{-1}; and the crossing probability is estimated to be only 2% at room temperature.

Once species **8** is formed, it would be followed by two possible pathways via methyl shift and methyl-H shift, respectively. Along the former pathway, facile β-C−C bond cleavage carries **8** into **3** via transition state **TS$_{8-3}$**, which assumes a much low energy barrier (lying at −35.1 (sextet) and −57.5 (quartet) kcal/mol). Direct dissociation of species **3** giving the energetic favorable CH_3 loss product $(HO)Fe^+(C_2H_4)$ has been discussed above.

Alternatively, a stepwise methyl-H shift, that is, methyl-H shift forming $(C_3H_6)Fe^+(H)(OH)$ species (**9**) (via transition state **TS$_{8-9}$**) and subsequent hydride H-shift (via **TS$_{9-10}$**), could carry species **8** into the $(C_3H_6)Fe^+(H_2O)$ complex (**10**). An obvious feature of species **10** is the four-member-ring (C^1, C^2, C^3, and Fe^+) structure, in which Fe^+ simultaneously attacks at both terminal C atoms of $CH_2CH_2CH_2$. NBO analysis of species **10** detects that in both states Fe^+ forms strong covalent bonds with $CH_2CH_2CH_2$ via doubly occupied $\sigma(Fe^+-C^1)$ and β-singly occupied $\sigma(Fe^+-C^3)$ bonding orbitals, whereas the binding of Fe^+-OH_2 is dominated by donor−acceptor stabilization and thus is relatively weak. As shown in Figure 4, the whole sextet PES is located highly above the quartet PES, whereas on the quartet PES the highest energy point (**^{4}TS$_{8-9}$**) lies at 29.8 kcal/mol below the energetic zero.

Different dissociation of **10** would account for $Fe^+ + c\text{-}C_3H_6 + H_2O$ (**P$_{2c}$**), $FeOH_2^+ + c\text{-}C_3H_6$ (**P$_{3b}$**), and $FeCH_2CH_2CH_2^+ + H_2O$ (**P$_{4b}$**), exothermic by −0.93 (−13.2), +31.1 (32.1), and +15.3 (35.6) kcal/mol in the sextet (quartet) state, respectively.

β,α-H Abstraction. PES together with schematic structures involved in the sextet and quartet pathways of the channel is shown in Figure 5. Information about these relevant species is given in Figures S5 (Supporting Information).

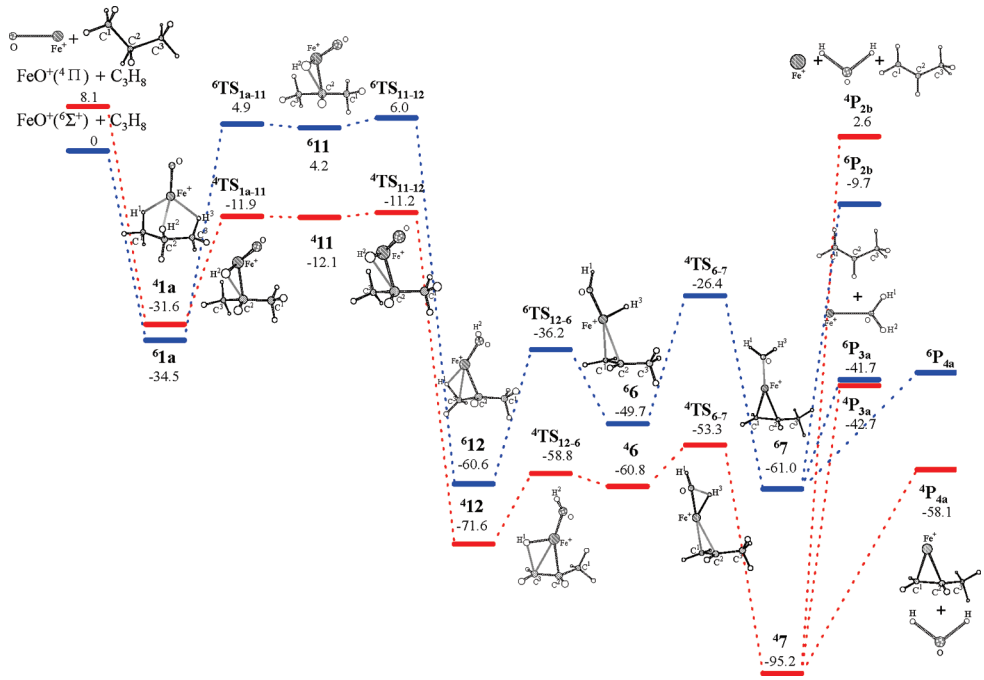

Figure 5. Energy profile the initial C−H activation channel following β,α-H abstraction involved in the reaction of FeO^+ with propane. Parameters follow the same notations as in Figure 2.

Occurring through encounter complex **1a**, this pathway involves a stepwise H shift from C^β to O, which includes a H shift from C^β to form the $(CH_3CHCH_3)Fe^+(H)(O)$ complex (**11**) and a hydride H-shift leading to $(CH_3CHCH_3)Fe^+(OH)$ complex **12**. The sextet pathway is identified as a high-energy channel because both the involved transition states (**^{6}TS$_{1a-11}$** and **^{6}TS$_{11-12}$**) and minimum **^{6}11** are located in a flat altiplano region (~5 kcal/mol above the entrance channel) on the PES, while the quartet channel is energetically favorable because all the involved stationary points (**^{4}TS$_{1a-11}$**, **^{4}TS$_{11-12}$**, and **^{4}11**) lie at 11.2−12.1 kcal/mol below the energetic zero. Energetically, species **12** is particularly stable, lying at 71.6 (60.6) kcal/mol below the energetic zero in its quartet (sextet) state. Indeed, it is the most stable species among all the analogous $(C_3H_7)Fe(OH)^+$ complexes (**4**, **8**, and **12**). A subsequent methyl-H shift in species **12** could result in hydride-containing species $(CH_2CHCH_3)Fe^+(H)(OH)$ (**6**), whose reactivity has been discussed above.

As shown in Figure 5, a sextet-to-quartet crossing is expected to occur before saddle point **TS$_{1a-11}$**. The activated C^β-H bond length in the relevant MECP$_{1a}$ is calculated to be 1.145 Å (see Figure S5, Supporting Information). The SOCC is calculated to be 418.0 cm^{-1}, and the intersystem crossing probability is estimated to be 83% at room temperature, indicating initial C^β−H activation accounts for a relatively large crossing probability, compared to initial C^α−H activation (MECP$_{1b}$ and MECP$_{1d}$).

3.3. Comparison with Experimental Results. In this section, we briefly compare our theoretical results with the findings from the gas-phase experiments by Jackson et al.[6] In the FTMS experiments, the reaction of FeO^+ with propane gives four different products, i.e., $FeC_3H_6^+$, $FeOH(C_2H_4)^+$, Fe^+, and $FeOH_2^+$ with a branching ratio of 0.5:0.2:0.2:0.1. These products can be classified as two groups: loss of a radical species (CH_3) and loss of closed-shell molecule (H_2O, C_3H_7OH, and C_3H_6).

In the present theoretical investigation, all possible pathways following initial C−C and C−H activation (including α,β-H, α,γ-H, and β,α-H abstraction) are searched for the reaction of FeO^+ with propane. Methyl loss product ($FeOH(C_2H_4)^+$), exothermic by 36.1 kcal/mol, could be produced via either the initial C−C activation or C−H activation (α,γ-H abstraction) (see Figures 2 and 4), while the initial C−H activation accounts for the H_2O, C_3H_7OH (H_2O + C_3H_6), and C_3H_6 elimination ($FeC_3H_6^+$, Fe^+, and $FeOH_2^+$) with 58.1, 13.8 (9.7), and 42.7 kcal/mol exothermicities, respectively (see Figures 3−5). In each case, there is a crossing between the high- and low-spin-state energy surfaces in the course of initial bond insertion (before the relevant transition state).

Although both initial C−C and C−H activation (α,γ-H abstraction) could be responsible for the elimination of CH_3 (see Figures 2 and 4), the former one is unlikely to be important because the transition states involved on both the quartet and sextet PESs are located much above the C−H activation PES and even above the entrance channel. Since the sextet-to-quartet crossing probability is very low (2%) in the course of the initial C^α−H activation from the 2α,2γ-η^4-$OFe^+(C_3H_8)$ complex (**1d**), the CH_3 elimination giving $FeOH(C_2H_4)^+$ (**P$_{1a}$**) is more likely to take place adiabatically on the sextet PES under the single-state reactivity (SSR) paradigm[32] (see Figure 4).

All three C−H activation channels could account for the H_2O, C_3H_6, and C_3H_7OH (H_2O + C_3H_6) loss products, but an inspection of the PESs shows that if the spin inversion is not considered, the α,β-H abstraction channel is the most favorable because it is not only simple (direct C^α-to-O H shift) but also energetically and dynamically favorable, whereas the other two (α,γ-H, and β,α-H abstraction) experience several high energy barriers (lying above the entrance channel) on the sextet PES. However, as mentioned above, the spin inversion in the course of the α,β-, β,α-, and α,γ-H abstraction results in the intersystem crossing probability of 74%, 88%, and 2%, respectively; thus the reactions via the α,β- and β,α-H abstraction mechanisms from the η^3 complexes (**1a**, **1b**, and **1c**) could proceed easily on the energetically favorable quartet surface (see Figures 3 and 5).

It can also be found from Figures 3−5 that the accompanying product of Fe^+ is C_3H_7OH rather than $H_2O + C_3H_6$, because loss of $H_2O + C_3H_6$ not only is less exothermic but also suffers from competition with the water and propylene losses at the exit. The loss of C_3H_7OH experiences a relatively simple pathway, which involves a direct C^α-to-O hydrogen shift from η^3-$OFe^+(C_3H_8)$ followed by the C−O coupling process.

The loss of H_2O producing $FeC_3H_6^+$ (**P$_{4a}$** and **P$_{4b}$**) is strongly favorable because of the strongest exothermicity as well as no high-lying transition states along the product pathway. Although the propene elimination product of $FeOH_2^+$ has a stronger exothermicity than the remaining two product channels (Fe^+ and $FeOH(C_2H_4)^+$), it should not be kinetically favorable due to the competition of the $FeC_3H_6^+ + H_2O$ channel at the exit. This situation agrees with the ICR experimental findings, in which the branching ratio of H_2O, C_3H_7OH, CH_3, and C_3H_6 losses was approximately determined to be 0.5:0.2:0.2:0.1.[6]

As is well-known, in propane, the C^α−H bond is a little stronger than the C^β−H bond (BDEs: 100.9 vs 98.1 kcal/mol[33]). However, the relative energies of the transition states suggest that the C^α−H bond activation in propane is preferred (see Figures 3−5). This behavior is counterintuitive but is in agreement with the theoretical results of propane/VO_2^+.[12d] Different structures of the transition states involved may provide a hint for this situation. For example, the C^α−H bond activation favors a concerted C^α-to-OH shift, and the involved transition states (**TS$_{1b-4}$**, **TS$_{1c-4}$**, **TS$_{1d-8}$**) are stabilized by the direct interaction between O and the shifting H, whereas in the C^β−H bond activation transition state (**TS$_{1a-11}$**), the stepwise C-to-O H shift predicts a very weak interaction between O and the shifting H.

4. Conclusions

The present theoretical work has helped us to gain further insight into the gas-phase reaction of FeO^+ with propane. Coordinations of the metal center of FeO^+ to α,β,γ-, 2α,β-, 3α-, and 2α,2γ-H atoms could account for four types of encounter complexes, i.e., three η^3- and one η^4-$OFe^+-C_3H_8$ complexes. All these complexes have the comparable stability reflected by the binding energies 31.1−36.7 (25.6−33.6) kcal/mol for the sextet (quartet) state. The reaction of FeO^+ with propane involves initial C−H activation in propane, while initial C−C bond scission is not important. The loss of a radical-type species (CH_3) in the reaction of FeO^+ with propane takes place adiabatically on the sextet PES via the simple C^α-to-O H shift from the η^4-$OFe^+(C_3H_8)$ complex followed by a CH_3 shift. For closed-shell molecule (C_3H_7OH, H_2O, and C_3H_6) elimination, all the three η^3-$OFe^+(C_3H_8)$ complexes could be involved. The C_3H_7OH elimination occurs through the direct C^α-to-O H shift from 2α,β- and 3α-η^3-$OFe^+(C_3H_8)$ (**1b** and **1c**) followed by C−O coupling on both the quartet and sextet PESs, while the loss of H_2O and C_3H_6 could take place via both the quartet and sextet pathways of α,β-H abstraction from **1b** and **1c** as well as the quartet β,α-H abstraction pathway from α,β,γ-η^3-$OFe^+(C_3H_8)$ (**1a**), in which spin−orbit coupling plays an important role.

Acknowledgment. This work was supported by Program for Changjiang Scholars and Innovative Research Team in University (IRT0759) of MOE, PRC, National Natural Science Foundation of China (10979077), CNPC Science & Technology Innovation Foundation (2009D-5006-04-07), and State Key Basic Research Program of PRC (2006CB202505).

Supporting Information Available: Optimized structures as well as selected structural parameters for all the intermediates, saddle points, and products involved in the oxidation of propane by FeO^+; calculated total energies, zero-point energies, and values of $\langle S^2 \rangle$ for all the relevant species. This material is available free of charge via the Internet at http://pubs.acs.org.

References and Notes

(1) (a) Torrent, M.; Solà, M.; Frenking, G. *Chem. Rev* **2000**, *100*, 439. (b) Niu, S.; Hall, M. B. *Chem. Rev.* **2000**, *100*, 353.

(2) Shilov, A. E.; Shul'pin, G. B. *Chem. Rev.* **1997**, *97*, 2879.

(3) Schröder, D.; Schwarz, H. *Angew. Chem., Int. Ed. Engl.* **1995**, *34*, 1973.

(4) Weisshaar, J. C. *Acc. Chem. Res.* **1993**, *26*, 213.

(5) (a) Böhme, D. K.; Schwarz, H. *Angew. Chem., Int. Ed.* **2005**, *44*, 2336. (b) Trage, C.; Schröder, D.; Schwarz, H. *Organometullics* **2003**, *22*, 693.

(6) Jackson, T. C.; Jacobson, D. B.; Freiser, B. S. *J. Am. Chem. Soc.* **1984**, *106*, 1252.

(7) Ryan, M. F.; Fiedler, A.; Schröder, D.; Schwarz, H. *J. Am. Chem. Soc.* **1995**, *117*, 2033.

(8) Kang, H.; Beauchamp, J. L. *J. Am. Chem. Soc.* **1986**, *108*, 7502.

(9) Ryan, M. F.; Fiedler, A.; Schröder, D.; Schwarz, H. *Organometullics* **1994**, *13*, 4072.

(10) Yoshizawa, K.; Shiota, Y.; Yamabe, T. *J. Am. Chem. Soc.* **1999**, *121*, 147.

(11) (a) Yoshizawa, K.; Shiota, Y.; Yamabe, T. *J. Am. Chem. Soc.* **1998**, *120*, 564. (b) Yoshizawa, K.; Shiota, Y.; Yamabe, T. *J. Chem. Phys.* **1999**, *111*, 538. (c) Shiota, Y.; Yoshizawa, K. *J. Am. Chem. Soc.* **2000**, *122*, 12317. (d) Shiota, Y.; Yoshizawa, K. *J. Chem. Phys.* **2003**, *118*, 5872. (e) Yoshizawa, K.; Shiota, Y.; Kagawa, Y.; Yamabe, T. *J. Phys. Chem. A* **2000**, *104*, 2552.

(12) (a) Shiota, Y.; Suzuki, K.; Yoshizawa, K. *Organometallics* **2005**, *24*, 3532. (b) Shiota, Y.; Yoshizawa, K. *Organometallics* **2001**, *20*, 1397. (c) Feyel, S.; Schröder, D.; Rozanska, X.; Sauer, J.; Schwarz, H. *Angew. Chem., Int. Ed. Engl.* **2006**, *45*, 4677. (d) Engeser, M.; Schlangen, M.; Schröder, D.; Schwarz, H. *Organometallics* **2003**, *22*, 3933. (e) Schröder, D.; Holthausen, M. C.; Kagawa, Y.; Schwarz, H. *J. Phys. Chem. B* **2004**, *108*, 14407. (f) Rozanska, X.; Sauer, J. *J. Phys. Chem. A* **2009**, *113*, 11586. (g) Rozanska, X.; Sauer, J. *Int. J. Quantum Chem.* **2008**, *108*, 2223.

(13) Zhao, L. M.; Wang, Y.; Guo, W. Y.; Shan, H. H.; Lu, X. Q.; Yang, T. F. *J. Phys. Chem. A* **2008**, *112*, 5676.

(14) Armentrout, P. B. *Top. Organomet. Chem.* **1999**, *4*, 1.

(15) Zhao, L. M.; Liu, Z. C.; Guo, W. Y.; Zhang, L. Z.; Zhang, F. Y.; Zhu, H. Y.; Shan, H. H. *Phys. Chem. Chem. Phys.* **2009**, *11*, 4219.

(16) Zhao, L. M.; Liu, Z. C.; Guo, W. Y.; Lu, X. Q.; Lin, X. Q.; Shan, H. H. *Chem. Phys. Lett.* **2008**, *463*, 54.

(17) (a) Stephens, P. J.; Devlin, F. J.; Chabalowski, C. F.; Frisch, M. J. *J. Phys. Chem.* **1994**, *98*, 11623. (b) Becke, A. D. *J. Chem. Phys.* **1993**, *98*, 5648. (c) Lee, C.; Yang, W.; Parr, R. G. *Phys. Rev. B* **1988**, *37*, 785. (d) Salahub, D. R. *The Challenge of d and f Electrons*; Zerner, M. C., Ed.; ACS: Washington, D.C., 1989. (e) Parr, R. G.; Yang, W. *Density-Functional Theory of Atoms and Molecules*; Oxford University Press: Oxford, U.K., 1989.

(18) Chiodo, S.; Russo, N.; Sicilia, E. *J. Comput. Chem.* **2005**, *26*, 175.

(19) Frisch, M. J.; Pople, J. A.; Binkley, J. S. *J. Chem. Phys.* **1984**, *80*, 3265.

(20) Rondinelli, F.; Russo, N.; Toscano, M. *Inorg. Chem.* **2007**, *46*, 7489.

(21) Schröder, D.; Schwarz, H. *J. Organomet. Chem.* **1995**, *504*, 123.

(22) (a) Gonzalez, C.; Schlegel, H. B. *J. Chem. Phys.* **1989**, *90*, 2154. (b) Gonzalez, C.; Schlegel, H. B. *J. Phys. Chem.* **1990**, *94*, 5523.

(23) (a) Seeger, R.; Pople, J. A. *J. Chem. Phys.* **1977**, *66*, 3045. (b) Bauernschmitt, R.; Ahlrichs, R. *J. Chem. Phys.* **1996**, *104*, 9047.

(24) (a) Glendening, E. D.; Reed, A. E.; Carpenter, J. E.; Weinhold, F. NBO, version 3.1. (b) Reed, A. E.; Curtiss, L. A.; Weinhold, F. *Chem. Rev.* **1988**, *88*, 899. (c) Foster, J. P.; Weinhold, F. *J. Am. Chem. Soc.* **1980**, *102*, 7211.

(25) Frisch, M. J.; Trucks, G. W.; Schlegel, H. B.; Scuseria, G. E.; Robb, M. A.; Cheeseman, J. R.; Montgomery, J. A., Jr.; Vreven, T.; Kudin, K. N.; Burant, J. C.; Millam, J. M.; Iyengar, S. S.; Tomasi, J.; Barone, V.; Mennucci, B.; Cossi, M.; Scalmani, G.; Rega, N.; Petersson, G. A.; Nakatsuji, H.; Hada, M.; Ehara, M.; Toyota, K.; Fukuda, R.; Hasegawa, J.; Ishida, M.; Nakajima, T.; Honda, Y.; Kitao, O.; Nakai, H.; Klene, M.; Li, X.; Knox, J. E.; Hratchian, H. P.; Cross, J. B.; Adamo, C.; Jaramillo, J.; Gomperts, R.; Stratmann, R. E.; Yazyev, O.; Austin, A. J.; Cammi, R.; Pomelli, C.; Ochterski, J. W.; Ayala, P. Y.; Morokuma, K.; Voth, G. A.; Salvador, P.; Dannenberg, J. J.; Zakrzewski, V. G.; Dapprich, S.; Daniels, A. D.; Strain, M. C.; Farkas, O.; Malick, D. K.; Rabuck, A. D.;

Raghavachari, K.; Foresman, J. B.; Ortiz, J. V.; Cui, Q.; Baboul, A. G.; Clifford, S.; Cioslowski, J.; Stefanov, B. B.; Liu, G.; Liashenko, A.; Piskorz, P.; Komaromi, I.; Martin, R. L.; Fox, D. J.; Keith, T.; Al-Laham, M. A.; Peng, C. Y.; Nanayakkara, A.; Challacombe, M.; Gill, P. M. W.; Johnson, B.; Chen, W.; Wong, M. W.; Gonzalez, C.; Pople, J. A. *Gaussian 03*, revision B.05; Gaussian, Inc.: Pittsburgh, PA, 2003.

(26) Schmidt, M. W.; Baldridge, K. K.; Boatz, J. A.; Elbert, S. T.; Gordon, M. S.; Jensen, J. H.; Koseki, S.; Matsunaga, N.; Nguyen, K. A.; Su, S. J.; Windus, T. L.; Dupuis, M.; Montgomery, J. A. *J. Comput. Chem.* **1993**, *14*, 1347.

(27) Matsunaga, N.; Koseki, S.; Gordon, M. S. *J. Chem. Phys.* **1996**, *104*, 7988.

(28) Fedorov, D. G.; Koseki, S.; Schmidt, M. W.; Gordon, M. S. *Int. Rev. Phys. Chem.* **2003**, *22*, 551.

(29) (a) Zener, C. *Proc. R. Soc. London, Ser. A* **1932**, *137*, 595. (b) Zener, C. *Proc. R. Soc. London, Ser. A* **1933**, *140*, 1174. (c) Fedorov, D. G.; Koseki, S.; Schmidt, M. W.; Gordon, M. S. *Int. Rev. Phys. Chem.* **2003**, *22*, 551.

(30) Schultz, R. H.; Armentrout, P. B. *J. Phys. Chem.* **1993**, *97*, 596.

(31) (a) Dewar, M. J. S. *Bull. Soc. Chim. Fr.* **1951**, *C79*, 18. (b) Chatt, J.; Duncansom, L. A. *J. Chem. Soc.* **1953**, 2939. (c) Gerloch, M.; Constable, E. C. *Transition Metal Chemistry*; VCH: New York, 1994; Chapter 6.5.

(32) (a) Harris, N.; Shaik, S.; Schröder, D.; Schwarz, H. *Helv. Chim. Acta* **1999**, *82*, 1784. (b) Schröder, D.; Shaik, S.; Schwarz, H. *Acc. Chem. Res.* **2000**, *33*, 139.

(33) Lias, S. G.; Bartmess, J. E.; Liebman, J. F.; Holmes, J. L.; Levin, R. D.; Mallard, W. G. *J. Phys. Ref. Data, Suppl.* **1988**, *17*, 1.

JP910774Z